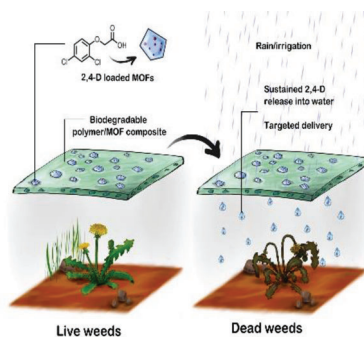R. A. dos Reis, L. A. M. Mahmoud,
E. H. Ivanovska, R. Telford,
M. A. Addicoat, L. R. Terry, V. P. Ting,
S. Nayak* 2300269

Biodegradable Polymer-Metal-Organic Framework (MOF) Composites for Controlled and Sustainable Pesticide Delivery

Biodegradable polymer-MOF composites are fabricated for controlled delivery of 2,4-dichloropheoxycetic acid (2,4-D) to reduce the amount of runoff and sustainable agriculture. Excellent loading of 2,4-D is achieved in the MOFs with up to 45 wt%, and a controlled delivery is observed over 16 days. Kinetics studies and computational modelling show a more controlled release for NH_2-functionalised MOF.

RESEARCH ARTICLE

Biodegradable Polymer-Metal-Organic Framework (MOF) Composites for Controlled and Sustainable Pesticide Delivery

Roberta A. dos Reis, Lila A. M. Mahmoud, Evdokiya H. Ivanovska, Richard Telford, Matthew A. Addicoat, Lui R. Terry, Valeska P. Ting, and Sanjit Nayak*

Due to high surface area, loading capacity, and selectivity, Metal-Organic Frameworks (MOFs) have shown much promise recently for potential applications in extraction and delivery of agrochemicals for environmental remediation and sustainable release, respectively. However, application of MOFs for pesticide delivery in wider agricultural context can be restricted by their granular form. Herein, an alternative approach is studied using biodegradable polymer-MOF composites to address this limitation. The loading and release of a widely used pesticide, 2,4-dichloropheoxycetic acid (2,4-D), is studied using two MOFs, UiO-66 and UiO-66-NH$_2$, and the 2,4-D-loaded MOFs are incorporated into biodegradable polycaprolactone composites for convenient handling and minimizing runoff. The MOFs are loaded by in-situ, and post-synthetic methods, and characterised thoroughly to ensure successful synthesis and loading of 2,4-D. The pesticide release studies are performed on the MOFs and composites in distilled water, and analysed using UV-Vis spectroscopy, demonstrating sustained-release of 2,4-D over 16 days. The loaded MOF samples show high loading capacity, with up to 45 wt% for the in-situ loaded UiO-66. Release kinetics show more sustained release of 2,4-D from UiO-66-NH$_2$ compared to UiO-66, which can be due to supramolecular interactions between the NH$_2$ group of UiO-66-NH$_2$ and 2,4-D. This is further supported by computational studies.

1. Introduction

The traditional application of pesticides results into large amounts of runoff chemicals that contaminate the environment, especially groundwater, and pose adverse effects on human health and the ecosystem.[1] Pesticides are a prevailing cause of habitat destruction, disruption of food webs, and an overall loss of biodiversity.[2] In humans, long-term pesticide exposure through contaminated water and foods have been linked to diseases including cancers, neuropathy, and immune system damage.[3] 2,4-dichlorophenoxyacetic acid (2,4-D) is a common active ingredient in most household weedkiller and lawn management products and widely used for broadleaf weed management.[4] However, its low water solubility can result in its bioaccumulation on plants and in soil, hence causing harm to the ecosystem by contaminating waterbodies through drift and runoff.[5] Studies have shown that pesticides are present in drinking water in varied concentrations across the globe, in all continents, including Antarctica.[6]

R. A. dos Reis, L. A. M. Mahmoud, E. H. Ivanovska, R. Telford, S. Nayak
School of Chemistry and Biosciences
University of Bradford
Bradford BD7 1DP, UK
E-mail: s.nayak@bradford.ac.uk

R. A. dos Reis
Centro de Ciências Naturais e Humanas
Universidade Federal do ABC
Santo André, SP 09.210-170, Brazil

L. A. M. Mahmoud
School of Pharmacy
Al-Zaytoonah University of Jordan
Amman 11733, Jordan

L. A. M. Mahmoud, L. R. Terry, V. P. Ting
Bristol Composites Institute
Department of Mechanical Engineering
University of Bristol
Bristol BS8 1TR, UK

M. A. Addicoat
School of Science and Technology
Nottingham Trent University
Clifton Lane, Nottingham NG11 8NS, UK

V. P. Ting
Research School of Chemistry & College of Engineering
Computing and Cybernetics
The Australian National University
Canberra ACT 2600, Australia

**ADVANCED
SCIENCE NEWS**

www.advancedsciencenews.com

**ADVANCED
SUSTAINABLE
SYSTEMS**

www.advsustainsys.com

The ubiquitous presence of pesticides in drinking water has prompted materials chemists to look for solutions for the remediation of soil and water from agrochemical contaminants, and some porous nanostructures, such as zeolites, silicates, porous carbon, and MXene, have shown promising results.[7] However, these materials are limited by their robust structures which are challenging to modify and functionalize chemically to induce any control over the interaction with the cargo molecules and on the release mechanism.[7b]

Metal-organic frameworks (MOFs) are a class of crystalline materials, formed by organic ligands coordinated to metal ions or cluster nodes, forming 2D or 3D networks with potential voids.[8] Following the first report of MOFs, by Yaghi et al. in 1995, there has been an explosion of interest in MOFs.[9] Due to their modular structure, tunability, high surface area, and high chemical stability,[10] MOFs have demonstrated high potential for applications in wide range of areas, such as hydrogen storage,[10] catalysis,[11] separation, and sensing.[10,12]

In recent studies, MOFs have also shown their potential vehicles for controlled drug delivery.[13] Controlled drug delivery ensures that the drug is slowly released over time, alleviating potential side effects and enhancing therapeutic efficacy.[14] The potential of MOFs for controlled delivery has recently been explored in the slow release of agrochemicals.[15] Since water is the key solvent for drug diffusion in vivo, the same model of diffusional release may be employed in pesticide delivery using MOFs, with the active molecule being released by the solvent interaction, in a typical diffusion-controlled mechanism.[13c] MOFs have proven to be excellent candidates for agricultural applications, particularly due to their high loading capacity, and controlled release over a longer period.[16,17] The first study using MOFs for slow release of agrochemicals was reported in 2015, for the controlled release of N and P fertilizers.[15c] Demonstrating their potential application in pesticide delivery, Yaghi et al. reported a controlled release of fumigant *cis*-1,3-dichloropropene using two calcium L-lactate MOFs, MOF-1203, and MOF-1201 in 2017.[18] Despite these promising results, the granular form of MOFs limits their scope for practical applications with a potential risk of releasing large amounts of MOFs into the environment. To address this limitation, an alternative approach was investigated in this study where two widely studied biocompatible and stable MOFs, UiO-66 and UiO-66-NH$_2$ were loaded with the chlorophenoxy pesticide, 2,4-D, and were integrated into biodegradable polymer matrix of polycaprolactone (PCL) membrane to allow easy handling and application in agricultural setup, as illustrated in **Scheme 1**.[15c,19] With successful fabrication of the composites and release studies showing an effective concentration of 2,4-D maintained over 16 days, a more sustainable contact-based approach for the delivery of pesticides using biodegradable MOF-polymer composites is reported here. As shown in Scheme 1, these composite membranes can find potential applications in controlled and targeted pesticide delivery triggered by irrigation or rain. This approach will facilitate delivery of the pesticide to the sites in contact with the weeds while minimizing pesticide contamination to non-targeted organisms and the surrounding environment. This approach will allow the composite membranes to be recovered and processed repurposed at the end of their applications, reducing the release of MOFs into the environment.
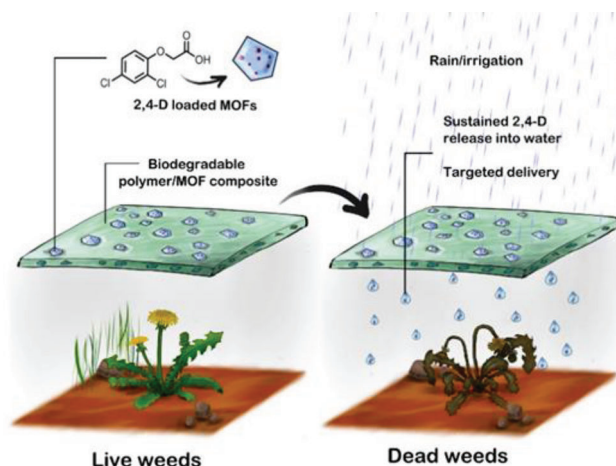
Scheme 1. Schematic showing potential application of Metal-organic framework (MOF)-polymer composites for the targeted and sustainable delivery of pesticides with possible reuse of the composite membranes.

2. Experimental Section

2.1. Synthesis

2.1.1. Materials Used

Zirconium(IV) tetrachloride (98%, anhydrous), terephthalic acid (98%), 2,4-D (analytical standard), and polycaprolactone with average molecular weight of 45 000, were purchased from Sigma-Aldrich. 2-aminoterephthalic acid (99%) was purchased from Thermo Scientific. All reagents and chemicals were analytical grade and were used without further purification. All solvents (HPLC grade) were obtained from Fisher Scientific. Deionized water was obtained through a Milli-Q Millipore purifying system (conductivity 18.2 MΩ cm).

2.1.2. Synthesis of Pristine UiO-66

In a 40 mL Teflon-lined glass vial 0.63 g (2.703 mmol) of zirconium tetrachloride (ZrCl$_4$) was added followed by addition of 5 mL of dimethylformamide (DMF). The mixture was sonicated for 20 min at 25 °C, followed by addition of 0.898 g (5.408 mmol) of benzene dicarboxylic acid (BDCA) and 10 mL of DMF along with 0.5 mL of conc. HCl. The closed vial was then placed in a programmable oven at 120 °C for 24 h with a heating rate of 10 °C per min, followed by cooling to 25 °C at a rate of 2 °C per minute. The white cloudy suspension was then filtered using vacuum filtration through a Buchner funnel. The resulting white crystalline solid was washed with fresh DMF and dried in a vacuum oven for 30 min. The solid yield: 86.5% with respect to ZrCl$_4$. IR (neat, cm^{-1}): 1660 (w), 1583 (m), 1507 (w), 1393 (s), 1257 (w), 1158 (w), 1101 (w), 1019 (w), 885 (w), 820 (w), 744 (s), 659 (s).

2.1.3. Synthesis of Pristine UiO-66

In a 40 mL Teflon-lined glass vial, 0.63 g (2.703 mmol) of ZrCl$_4$ was added to 5 mL of DMF and 0.5 mL of HCl. The vial was

**ADVANCED
SCIENCE NEWS**

www.advancedsciencenews.com

**ADVANCED
SUSTAINABLE
SYSTEMS**

www.advsustainsys.com

sonicated for 20 min at 25 °C, followed by addition of 0.979 g (5.408 mmol) of 2-aminobenzenedicarboxylic acid and 10 mL of DMF. The vial was placed in a programmable oven at 120 °C for 24 h with a heating rate of 10 °C per minute and a cooling rate of 0.5 °C per minute. The resultant cloudy suspension was filtered through a Buchner funnel via vacuum filtration. The yielded yellow crystalline solid was washed thoroughly with DMF and dried for 30 min. The yield: 63.9% with respect to $ZrCl_4$. IR (neat, cm^{-1}): 3464 (b), 3350 (b), 1654 (s), 1569 (s), 1495 (m), 1433 (s), 1385 (s), 1339 (m), 1260 (m), 1158 (w), 1101 (w), 970 (w), 894 (w), 823 (w), 798 (w), 766 (m), 656 (s).

2.1.4. Synthesis of UiO-66 with In Situ Loading of 2,4-D (IS-2,4-D@UiO-66)

In a 40 mL Teflon-lined glass vial, 0.63 g (2.703 mmol) of $ZrCl_4$ and (5.408 mmol) of BDCA were added along with 15 mL of DMF and 1.33 g (6.017 mmol) of 2,4-D. The vial was sonicated for 20 min at 25 °C and placed in programmable oven at 120 °C for 24 h with a heating rate of 10 °C per minute and cooling rate of 0.5 °C per minute. The resultant white suspension was vacuum filtered using a Buchner funnel and the resultant white powder was washed thoroughly with DMF, and dried in vacuum oven for 24 h. IS-2,4-D@UiO-66–567 mg. IR (neat, cm^{-1}): 1701 (w), 1587 (m), 1506 (w), 1478 (w), 1397 (s), 1291 (w), 1265 (w), 1234 (w), 1158 (w), 1105 (w), 1078 (w),1017 (w), 885 (w), 864 (w), 820 (w), and 745 (s).

2.1.5. Synthesis of UiO-66-NH$_2$ with In Situ Loading of 2,4-D (IS-2,4-D@UiO-66-NH$_2$)

In a 40 mL Teflon-lined glass vial, 0.63 g (2.703 mmol) of $ZrCl_4$ and, 0.979 g (5.408 mmol) of 2-aminoterephthalic acid were added along with 15 mL of DMF and 2.66 g (12.035 mmol) of 2,4-D. The vial was sonicated for 20 min at 25 °C and placed in programmable oven at 120 °C for 24 h with a heating rate of 10 °C per minute and a cooling rate of 0.5 °C per minute. The resultant suspension was vacuum filtered via Buchner funnel and dried at oven at 60 °C for 15 min. The resultant yellow powder was washed thoroughly with DMF, and dried in vacuum oven for 24 h. IS-2,4-D@UiO-66- NH_2–52,2 mg. IR (neat, cm^{-1}): 3464 (b), 3350 (b), 1699 (m), 1656 (m), 1578 (m), 1526 (s), 1481 (s), 1431(m), 1383 (s), 1392 (m), 1320(w), 1266 (m), 1234 (s), 1150 (s), 1123 (w), 1103(s), 1078(s),1042(s), 951(s),911 (s), 868 (m), 851 (w), 825 (w), 802 (s).767 (w), 753 (m).

2.1.6. Solvent Exchange and Activation of MOFs

Prior to post-synthetic loading of 2,4-D into UiO-66 and UiO-66- NH_2, solvent exchange was carried out first washing the MOFs with 15 mL of MeOH for 20 min and then collecting the solid by centrifuging at 4600 rpm.The resulting solid was left into 15 mL of DMF for solvent exchange for 24 h followed by filtration and drying the MOF samples at 150 °C for 24 h in a vacuum oven. The phase purity was confirmed by PXRD and no further purification were performed for the pristine MOFs and 2,4-D loaded MOFs.

2.1.7. Post-Synthetic Loading of 2,4-D (PS-2,4-D@UiO-66 and PS-2,4-D@UiO-66-NH$_2$)

In a 250 mL round bottom flask, a stock solution was prepared by dissolving 1.33 g (6.017 mmol) of 2,4-D in 100 mL of ethanol. For loading, 10 mL of 2,4-D solution was transferred to a 50 mL round bottom flask and 0.05 g of pristine MOF was added. The mixture was stirred for 48 h at room temperature at 900 rpm in a closed round bottomed flask. The MOF was recovered by centrifugation and washed with EtOH (3 × 10 mL–20 min at 4600 rpm by centrifuge). The resulting solid was dried into a vacuum oven for 24 h at 80 °C.

2.1.8. Preparation of Polycaprolactone-MOF Composites

In a 50 mL round bottom flask, 200 mg of polycaprolactone polymer (PCL) was added to 15 mL chloroform. The mixture was stirred until the polymer was completely dissolved. In a small beaker, 5 mL of the resulting solution was added to 5 mg of MOF powder and stirred for 30 min at room temperature. The solution was casted into a silicon mold and was left to dry at room temperature, to yield polymer-composite sheets that could be peeled off to collect from the mold.

2.1.9. Computational Method

2,4-D (n = 1,2) and water (n = 1) molecules were inserted stochastically into methyl-capped tetrahedral and octahedral pores of UiO-66 and UiO-66- NH_2 using the Kick3 stochastic structure generator.[20] Initial geometries were pre-optimized using UFF4MOF fixing the Zr atoms in their crystallographic positions,[21] before optimization with GFN1-xTB[22] as implemented in AMS2022.[23] For UiO-66- NH_2, the process was repeated three times employing different isomers (with respect to the positions of the NH_2 groups). Binding energies of 2,4-D and water within the MOF pores were calculated from the final GFN1-xTB optimized geometries by: BE = E(mol@MOF) − [E(MOF) + E(mol)].

2.2. 2,4-D Release Studies

$$C_t^{Cuvette} = \frac{A^{232\,nm} - 0.04761}{7797.4} \quad (1)$$

$$C_t^{Sample} = 3 * C_t^{Cuvette} \quad (2)$$

$$C_t^{Stock} = C_t^{Sample} + 0.1 * \sum_{Ct = 0}^{t-1} C_t^{Sample} \quad (3)$$

Adapted from Neyadi et al.,[13c] 5 mg of MOFs was added in 30 mL deionized at room temperature and left in a closed round bottomed flask. For each sample collection at different time intervals, 3 mL of the solution was taken out at set time and replaced by 3 mL of deionized water to maintain the constant volume. Sample (1 mL) was added to a quartz cuvette with 2 mL of water for UV–vis analyzes. Two absorption peaks at 232 and

**ADVANCED
SCIENCE NEWS**

www.advancedsciencenews.com

**ADVANCED
SUSTAINABLE
SYSTEMS**

www.advsustainsys.com

289 nm were identified for 2,4-D and used to determine the concentration of 2,4-D at various time intervals. Equations 1–3 were used (where C_t^{Stock} is the corrected concentration at time t, C_t^{Sample} is the estimated pesticide concentration at time t, $C_t^{Cuvette}$ is the concentration calculated from absorption directly at time t). All the absorption data measured three times.

For polymer composites, 10 mg of the dried polymer matrix or dried powder polymer-MOF composite was added in 30 mL distilled water at room temperature. The solution was then left static for 16 days at room temperature in a closed round bottomed flask. Solution (3 mL) was taken out each time and rapidly replaced with the same quantity of distilled water. A UV–vis spectrophotometer set to 332 nm was used to determine the quantity of pesticide released from MOF. The calibration curve was used to calculate the concentration of pesticide in water (Section S1, Supporting Information) using the Equations 4 and 5.

$$C_t^{Cuvette} = \frac{A^{232nm} - 0.04761}{7797.4} \quad (4)$$

$$C_t^{Stock} = C_t^{cuvette} + 0.1 * \sum_{Ct=0}^{t-1} C_t^{cuvette} \quad (5)$$

2.3. Loading Capacity

Loading capacity was determined using a modified method from literature.[24] MOFs (5 mg) were suspended into 3 mL of distilled water. The suspension was sonicated in a bath for 30 min. Then, the concentration was measured using a UV–vis spectrophotometer by taking 1 mL aliquot of solution and diluting with 2 mL of water. The mass of 2,4-D released was determined from the volume, and the loading capacity in percentage was calculated using Equation 6:

$$\text{Loading capacity } (\%) = \frac{\text{mass of } 2,4-D}{\text{mass of MOF}} * 100 \quad (6)$$

2.4. Instruments and Characterization

Fourier-Transformed Infrared (FTIR) spectra were recorded over the range of 600–4000 cm^{-1} using a PerkinElmer Spectrum 100 FTIR spectrometer fitted with a PerkinElmer Universal ATR sampling device. Thermogravimetric analyzes (TGA) were carried out using a Q5000IR thermogravimetric analyzer (TA Instruments, USA). Samples (ca. 5 mg) were placed in a platinum pan and heated from 30 to 600 °C at a ramp of 5 °C min^{-1} under nitrogen purge gas flow of 25 mL min^{-1}. TA Instruments Universal AnalysIS000 software was employed to process the data. SEM images and energy dispersive X-ray (EDX) elemental analysis data were collected using an FEI Quanta 400 E-SEM instrument fitted with an Oxford Xplore30 EDS system. The samples were sputter-coated with gold using an Emitech K550 coating system and the analyzes were carried out under vacuum. Powder X-ray diffraction (PXRD) data were collected at ambient temperature using a Bruker D8 diffractometer with Cu K$\alpha_{1,2}$-radiation ($\lambda = 0.154\,018$ nm, 1600 W) source. Quartz cuvettes (Hellma, QS Suprasil) had a volume of 3.0 mL and an
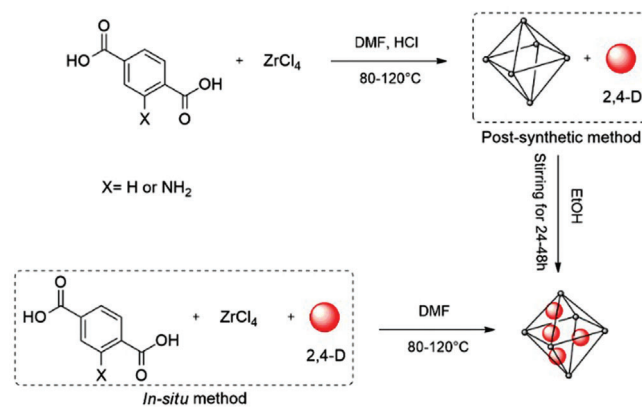
Scheme 2. Schematic illustration of the synthesis of UiO-66 and UiO-66-NH$_2$ and loading of 2,4-D using post-synthetic and in situ methods.

optical path of 10.00 mm, with two polished sides for absorption. The absorption analyzes were recorded on a Jenway UV–vis spectrophotometer—7205 model at 232 nm and/or 289 nm using quartz cuvettes (Hellma, QS Suprasil) with a volume of 3.0 mL and an optical path length of 10.00 mm. All the measurements were performed at room temperature and at atmospheric pressure. Electrospray ionization Mass Spectra (ESI-MS) were recorded using a Thermo Orbitrap LTQ (Thermo Fisher Scientific, UK) equipped with an electrospray ionization source operating in negative mode, with a sample dissolved in methanol and injected at 10 µL min^{-1} using the embedded syringe pump.

For surface area analysis, information on the specific surface area and internal pore structure was obtained from N$_2$ adsorption at 77 K on a Micromeritics 3Flex volumetric gas sorption analyser. Each material ($\approx$10–25 mg) was degassed prior to the experiment (388 K, $\approx$8 h, 1×10^{-6} mbar). Helium was used for free-space determination following isothermal data collection. N$_2$ and helium were supplied by Air Liquide and of purity 99.999%. Pore volume distribution as a function of pore width was calculated from the N$_2$ adsorption data (up to 0.94 P/P_0) using a density functional theory (DFT) fitting and a cylindrical pore—NLDFT Tarazona Esf = 30 K model. The BET surface area was determined following the procedure outlined in ISO 9277. A Rouquerol correction[25] was applied to the BET fitting to calculate surface areas. A resultant correlation function of > 0.9999 was observed for each material and a positive intercept (Figure S3, Supporting Information).

3. Results and Discussion

In this study, two stable and biocompatible MOFs, UiO-66 and UiO-66-NH$_2$, were synthesized by solvothermal method using DMF, and the resulting solids were activated by washing with methanol and DMF, followed by vacuum drying at 150 °C. Loading of 2,4-D into activated UiO-66 and UiO-66-NH$_2$ were carried out using post-synthetic and in situ method (**Scheme 2**), followed by their incorporation into biodegradable polycaprolactone membranes that were studied for release of 2,4-D over a period of 16 days in aqueous medium. For post-synthetic loading, the duration of loading (48 h) was decided based on optimization, as no further increase in loading was observed beyond 48 h of loading.
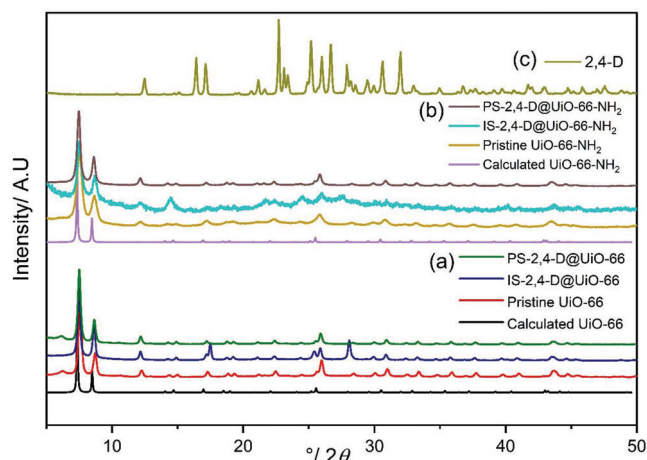
ADVANCED
SCIENCE NEWS

www.advancedsciencenews.com

ADVANCED
SUSTAINABLE
SYSTEMS

www.advsustainsys.com

Figure 1. PXRD patterns of a) calculated and pristine UiO-66, in situ and post-synthetically 2,4-D loaded UiO-66 and b) calculated and pristine UiO-66-NH$_2$, in situ and post-synthetically 2,4-D loaded UiO-66-NH$_2$, and c) 2,4-D, are shown.

3.1. Characterization of MOFs

The MOF samples were characterized using PXRD, TGA, FT-IR, SEM, and BET surface area analyses. As shown on **Figure 1**, all synthesized MOF samples are phase pure and the characteristic Bragg diffraction peaks are comparable to the calculated X-ray diffraction patterns of UiO-66 and UiO-66-NH$_2$.[26] The 2,4-D loaded MOFs did not show any additional peaks indicating that the MOFs retained their crystalline structure, without any degradation or impurities.

The FTIR spectra of UiO-66 and UiO-66-NH$_2$ MOFs are in agreement with literature (**Figure 2**).[5a,27] In all samples, two sharp peaks observed ≈1580 and 1390 cm^{-1} can be attributed to asymmetric and symmetric stretching vibrations of the OCO group of the linker. At lower frequencies, bands observed ≈760–740 and 684 cm^{-1}, can be assigned to C–H bending and μ_3-O
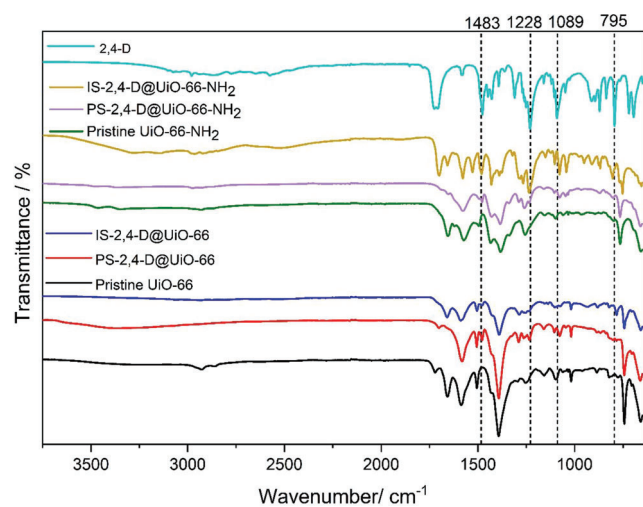

Figure 2. FTIR spectra of 2,4-D, pristine, and in situ and post-synthetically loaded UiO-66 and UiO-66-NH$_2$ MOFs.

stretch, respectively. For UiO-66-NH$_2$, broad peaks observed at 3300 and 3500 cm^{-1} correlate to the asymmetric and symmetric N–H bond stretching, in addition to the band at 1433 cm^{-1} due to the N–H stretch. For loaded MOFs, the presence of 2,4-D can be observed in bands indicating the C–Cl stretch at 795 cm^{-1}. For post-synthetic loaded samples, the peaks originating from 2,4-D can be found at 1089 and 1228 cm^{-1} (C–O–C, ester), and 1483 cm^{-1} for CH$_2$ (Figure 2).

Thermogravimetric analyzes (TGA) for all samples were investigated and are shown in **Figure 3**. All MOF samples exhibit three steps of weight-loss. The first weight-loss occurs between 50 and 150 °C represents the loss of trapped solvent molecules, followed by a second step observed starting from 125 to 305 °C can be attributed to the decomposition of the organic linker and the dehydroxylation of Zr-oxo clusters.[28] The loaded samples showed another step of weight loss between 175 and 380 °C, and this can be attributed to the decomposition of 2,4-D.[29] The final weight-loss occurs between 400 and 600 °C indicating the total degradation of the MOF.

The morphology of the samples were checked by scanning electron microscopy (SEM) and homogeneity were confirmed, as shown in **Figure 4**. This is in agreement with the PXRD which indicates single phase of the materials, without any visible impurity. The post-synthetically loaded MOFs maintained their morphology after loading with 2,4-D. In agreement with literature, the octahedral shapes of the UiO-66 crystals can be observed, and the size of the crystals appeared smaller for UiO-66-NH$_2$ and its derivatives compared to UiO-66 and its 2,4-D-loaded analogues.[30]

3.2. Surface Area Analysis

N$_2$ gas sorption experiments were carried out on each material to determine surface area, pore volume and pore size distribution. Adsorption–desorption N$_2$ isotherms of the 2,4-D doped MOFs are compared against pristine UiO-66 and UiO-66-NH$_2$ measured previously[15c] (**Figure 5**). As classified by IUPAC,[25] all 2,4-D doped UiO-66 MOFs exhibit Type I isotherms indicating microporous materials, with uptake governed by micropore volume. IS-2,4-D@UiO-66 also exhibits a degree of meso/macropore uptake indicated at pressures >0.9 P/P_0. This may be due to particulate size and packing, creating large inter-particulate voids or possible degradation of the crystal and pore network during the doping process. For 2,4-D loaded UiO-66-NH$_2$ MOFs, Type I isotherms with an increased level of meso/macropore uptake at the highest pressures were observed for all samples. This may be due to particulate size and packing, creating larger inter-particulate voids, but also could indicate degradation of the crystal and pore network during the doping process.

To calculate surface area, BET plots were taken for each sample (Figure S3, Supporting Information) and fitted using the Rouquerol method, ensuring a positive y-intercept and the highest correlation function (R2) values. **Table 1** summarizes the calculated pore characteristics of the MOF samples compared against pristine UiO-66 and UiO-66-NH$_2$ previously measured1. In comparison to the pristine UiO-66 MOF, all 2,4-D doped UiO-66 MOFs exhibited a reduced total quantity of adsorbed N$_2$, indicating a loss in porosity for the samples, as reflected by the
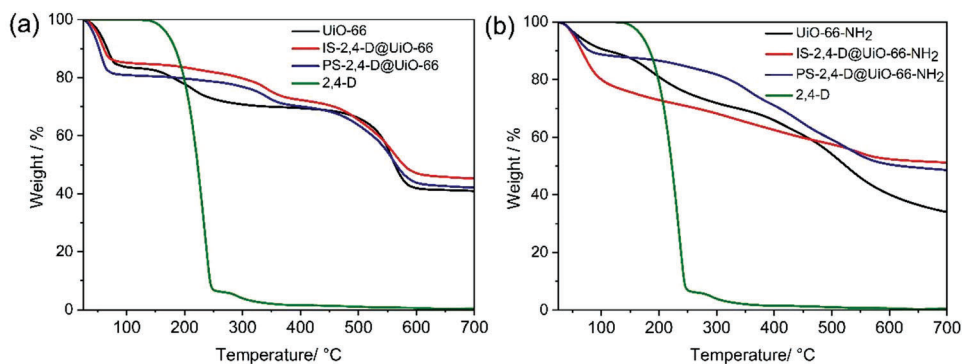
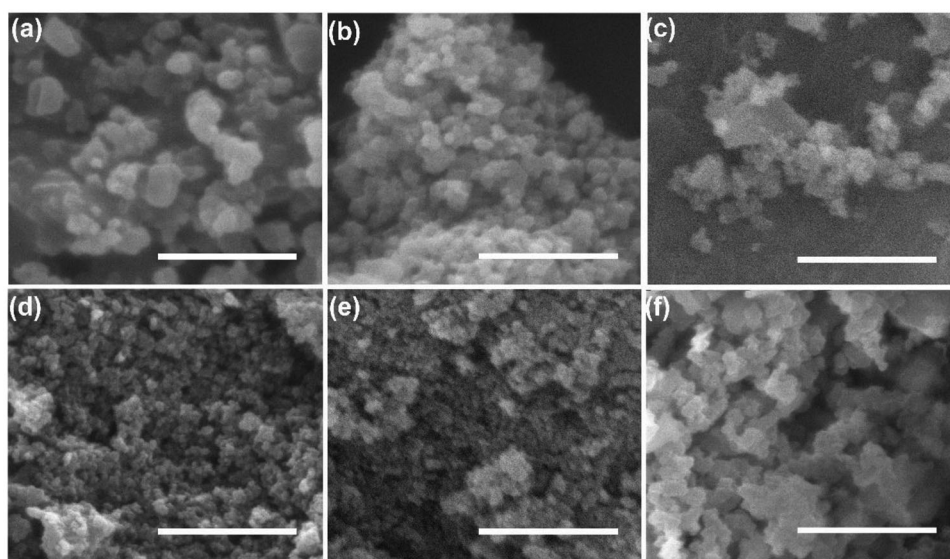**Figure 3.** TGA plots for a) UiO-66 samples and b) UiO-66-NH$_2$ samples.

Figure 4. SEM images of MOF samples: a) Pristine UiO-66 b) PS-2,4-D@UiO-66 c) IS-2,4-D@UiO-66 d) Pristine UiO-66-NH$_2$ e) PS-2,4-D@UiO-66-NH$_2$ f) IS-2,4-D@UiO-66-NH$_2$. Scale bars: 2 µm.
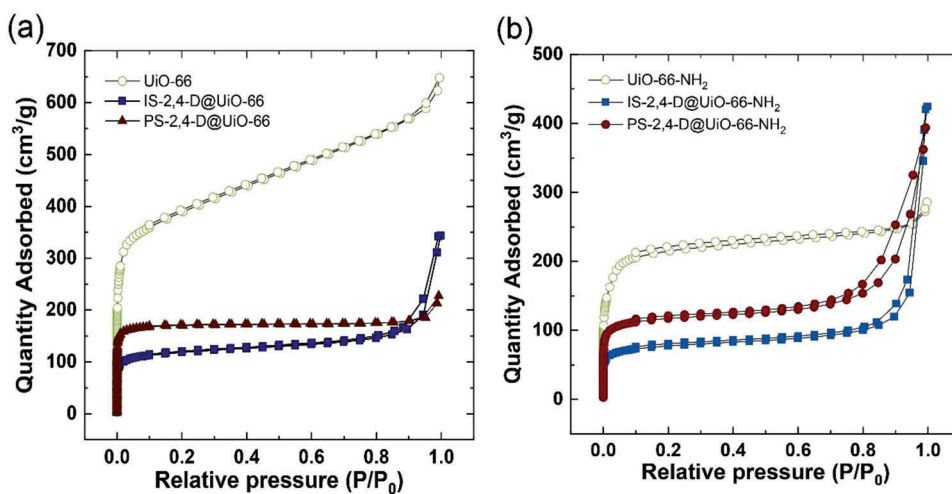

Figure 5. Nitrogen adsorption–desorption isotherms of a) UiO-66 and 2,4-D loaded UiO-66, and b) UiO-66-NH$_2$ and 2,4-D loaded UiO-66-NH$_2$ are shown.

**ADVANCED
SCIENCE NEWS**

www.advancedsciencenews.com

**ADVANCED
SUSTAINABLE
SYSTEMS**

www.advsustainsys.com

Table 1. Surface area, pore volume and pore size characteristics of MOF samples.

Sample	BET Surface Area [$m^2\ g^{-1}$]	Total Pore Volume[a] [$cm^3\ g^{-1}$]	Micro and mesopore Volume[b] [$cm^3\ g^{-1}$]	Modal Pore Size [Å]
UiO-66	1455.7 ± 2.19	0.913	0.724	5.9
IS-2,4-D @UiO-66	451.8 ± 0.52	0.295	0.215	5.9
PS-2,4-D @UiO-66	689.3 ± 0.19	0.288	0.300	7.7
UiO-66-NH$_2$	865.2 ± 5.91	0.394	0.383	5.9
IS-2,4-D@UiO-66-NH$_2$	293.2 ± 0.52	0.266	0.134	5.9
PS-2,4-D@UiO-66-NH$_2$	520.1 ± 0.49	0.411	0.242	5.9

[a] Single point adsorption volume taken at P/P_0 0.94; [b] DFT cumulative pore volume of pores < 50 Å.

diminished surface area (SA) and total pore volume (TPV) observed for the samples. IS-2,4-D@UiO-66 observed a 69% reduction in SA and a 68% reduction in TPV. While PS-2,4-D@UiO-66 observed a 53% reduction in SA and a 68% reduction in TPV. In comparison to the pristine UiO-66-NH$_2$ MOF, all 2,4-D doped UiO-66-NH$_2$ MOFs exhibited a slightly higher total quantity of

adsorbed N$_2$, due to the increased meso/macropore content observed at higher pressures. However, all samples experienced a reduced surface area, indicating a loss in microporosity, however, only IS-2,4-D@UiO-66-NH$_2$ experienced a reduction in total pore volume. whereas post-synthetic loaded MOFs experienced an increase in total pore volume.
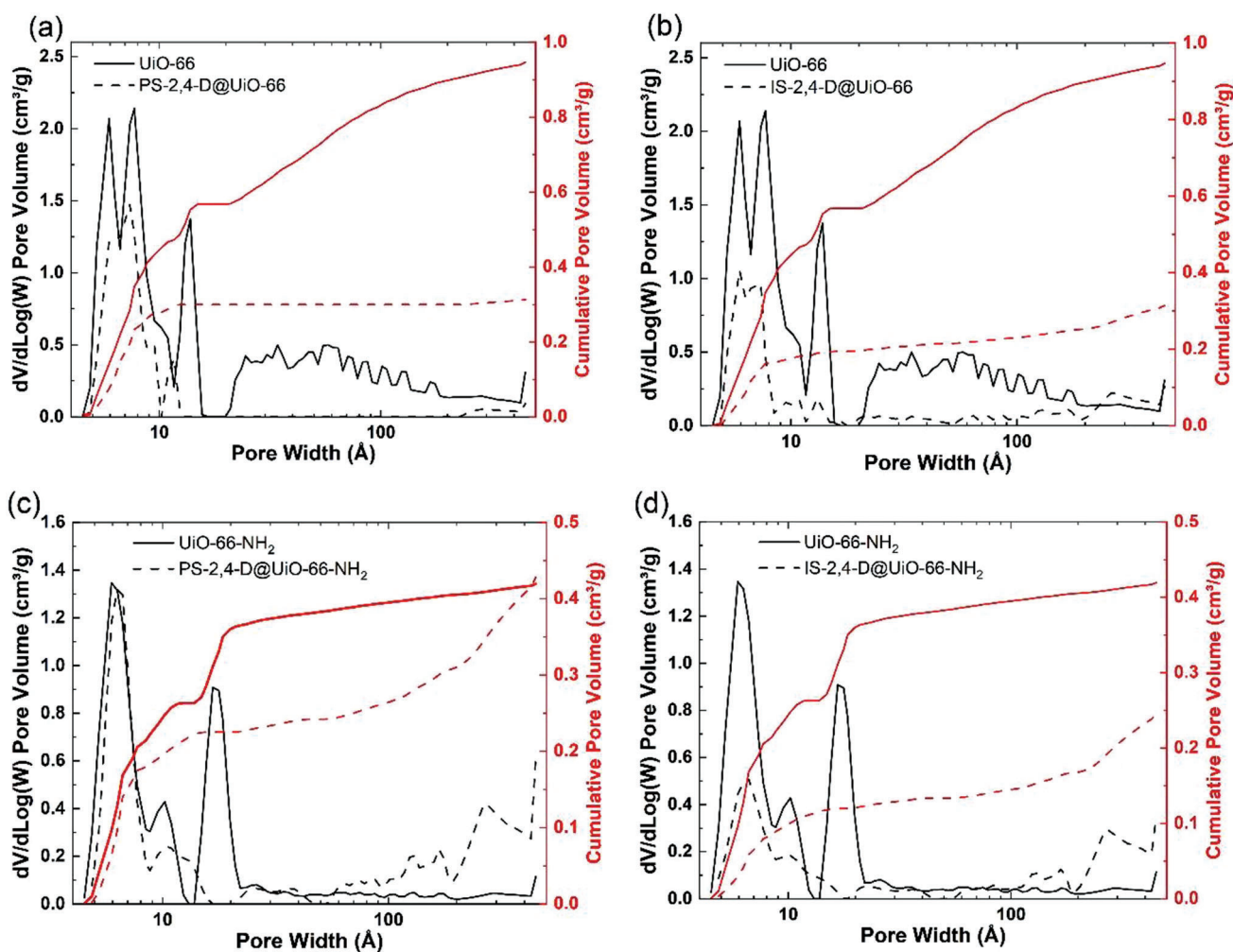

Figure 6. a-d) Pore size distribution and cumulative pore volume of pristine MOFs and 2,4-D loaded MOF samples, fitted with a Tarazona cylindrical pore NLDFT model.

**ADVANCED
SCIENCE NEWS**

www.advancedsciencenews.com

**ADVANCED
SUSTAINABLE
SYSTEMS**

www.advsustainsys.com

IS-2,4-D@UiO-66-NH$_2$ observed a 66% reduction in SA and a 32% reduction in TPV, while PS-2,4-D@UiO-66-NH$_2$ showed a 40% reduction in SA and a 4% increase in TPV.

Observed reductions in the surface area could be due to either guest molecules occupying available pores or degradation of the original pore network. The morphology of the samples were checked by scanning electron microscopy (SEM) and homogeneity were confirmed, as shown in.

Analysis of the calculated pore size distributions and the cumulative pore volumes implies changes to the pore network and available pore volume in the samples, revealing if pores are occupied/ blocked with molecules or if any changes of the network have occurred during processing. Pore size distributions and cumulative pore volume of samples were calculated by fitting the isotherms to DFT models, with the Tarazona cylindrical pore NLDFT model achieving the best goodness of fit. Results for the 2,4-D doped UiO-66 and UiO-66-NH$_2$ MOFs were compared to pristine UiO-66 and UiO-66-NH$_2$ (**Figure 6**).

When the 2,4-D doped UiO-66 MOFs were compared to the pristine UiO-66 MOF, a substantial loss of available pore volume for pore sizes >20 Å was noticed, with in situ samples retaining some of the mesoporosity. This could imply that the 2,4-D molecule sits inside these pores. For pore sizes <20 Å, a reduction in available pore volume is also observed, with the most significant loss to pores with diameters ≈13.8 Å, suggesting the 2,4-D molecule chiefly resides in this pore. Loss of available volume in smaller pores (5.9 and 10.2 Å) could be due to either the 2,4-D molecule sitting in these pores or access to these pores being blocked. For IS-2,4-D@UiO-66, the available pore volume in pore sizes 5.9 and 7.7 Å are reduced by ≈49% and ≈55% respectively, whereas pore volume in pore size 13.8 Å reduced by ≈86%. For PS-2,4-D@UiO-66, available pore volumes in pore sizes 5.9 and 7.7 Å are reduced by 41% and 31% respectively. Interestingly the original 13.8 Å sized pore in UiO-66, no longer exists and a new pore sized ≈11.7 Å is observed with an available pore volume at 30% of the capacity of the original. When the 2,4-D doped UiO-66-NH$_2$ MOFs were compared to the pristine UiO-66 MOF-NH$_2$, a substantial gain in available pore volume from pore sizes >100 Å was observed, with post-synthetic sample exhibiting the largest gains. The increase in mesoporosity observed in the DFT PSDs indicates the formation of new pores in the samples. For pore sizes <20 Å, the major reduction in available pore volume is caused by the loss of available volume in pores sized 16.7 Å, suggesting the 2,4-D molecule resides chiefly resides in this pore. Loss of available volume in smaller pores (5.9 and 10.2 Å) could be due to either the 2,4-D molecule sitting in these pores or access to these pores is being blocked. For IS-2,4-D@UiO-66-NH$_2$, the available volume for pores >100 Å increased by 416%. Available pore volume in pore sizes 5.9 and 10.2 Å reduced by 62% and 57% respectively. The original 16.7 Å sized pore in UiO-66-NH$_2$ no longer exists, indicating that it may be filled with guest molecules. A smaller shoulder is observed at 13.8 Å, with an available pore volume at 10% capacity of the original 16.7 Å sized pore. For PS-2,4-D@UiO-66-NH$_2$, the available volume for pores >100 Å increased by 674%. Available pore volume in pore size 5.9 Å remained equivalent to that of the pristine UiO-66-NH$_2$ MOF. The available pore volume in the pore sized 10.2 Å was reduced by 43%. The original 16.7 Å sized pore in UiO-66-NH$_2$ no longer exists and a new pore sized 13.1 Å, is observed,
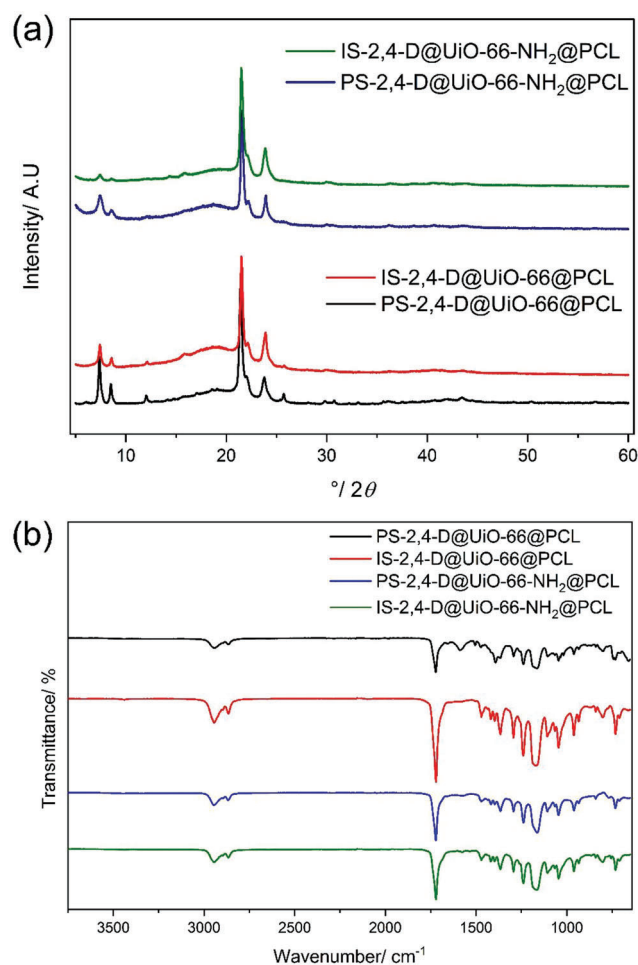

Figure 7. a) PXRD and b) FTIR spectra of 2,4-D loaded MOF-PCL composites.

with an available pore volume at 20% capacity of the original 16.7 Å sized pore.

3.3. Polycaprolactone-MOF Composites

The incorporation of pesticide-loaded MOFs into a biocompatible and biodegradable polymer will enable integrating them into sheet membranes that can be used and recycled for sustainable delivery various agrochemicals. To study the viability, all the 2,4-D loaded MOFs were integrated into PCL composite. The PCL-MOF composites (**Figure 7**) were characterized using PXRD, TGA, FT-IR and SEM.

FTIR analyzes performed on the composites show characteristic peaks at 2941 cm^{-1} for C—C bond stretching and at 1791 cm^{-1} originating from the C=O stretching of PCL. PXRD patterns of the composites show characteristic peaks of the MOFs, confirming that no phase changes occurred during the preparation of the composites. Diffraction peaks at 22° and 25° (2Θ) correspond to the crystallinity of the polymer structure for the PCL composite, while the peaks between 5 and 10° are from the UiO-66 and UiO-66-NH$_2$ in the composite (Figure 5), and their low intensities indicate the small proportion of the MOFs present in

**ADVANCED
SCIENCE NEWS**

www.advancedsciencenews.com

**ADVANCED
SUSTAINABLE
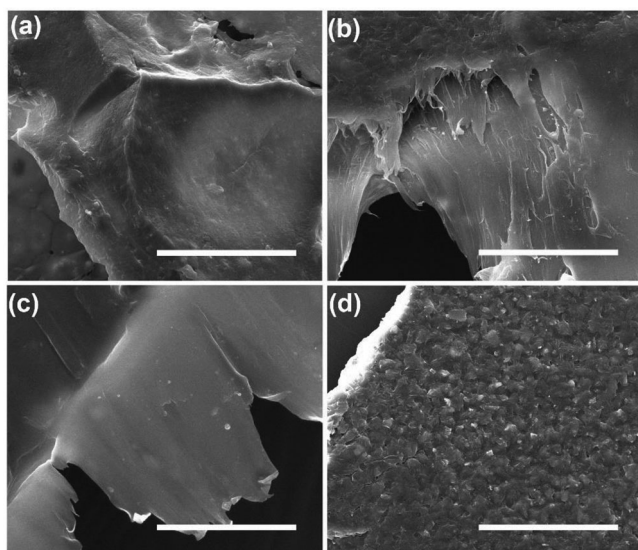SYSTEMS**

www.advsustainsys.com

Figure 8. SEM images of polymer-MOF composites of a) PS-2,4-D@UiO-66, scale bar is 100 μm b) IS-2,4-D@UiO-66, scale bar is 50 μm c) PS-2,4-D@UiO-66-NH$_2$, scale bar is 100 μm d) IS-2,4-D@UiO-66-NH$_2$, scale bar is 20 μm.

the composites. From the TGA (Section S4, Supporting Information), all polymer composite samples showed a significant loss in weight percentage ($\geq$ 90%), with first weight loss (between 250 and 260 °C) which can be attributed to the degradation of PCL.[31] SEM imaging of the composites showed well dispersed particulate microcrystalline MOFs in the polymer matrix (**Figure 8**).

3.4. Loading and Pesticide Release Studies

Presence of 2,4-D in the loaded UiO-66 and UiO-66-NH$_2$ were confirmed by electrospray ionization mass spectroscopy (ESI-MS) of the release medium after sonicating the 2,4-D loaded MOFs in distilled water for an hour. The ESI-MS spectra showed distinct peak at 219 (m/z) corresponding to deprotonated 2,4-D (Section S3, Supporting Information) molecules all loaded MOFs.

Time-dependent pesticide release studies were performed in water over a period of 16 days. As shown in Figure 7, the concentration of 2,4-D increased steadily up to day 4 (96 h) reaching equilibrium, and maintaining a stable concentration for the following 12 consecutive days. Since MOFs are stable in the conditions of this study,[32] it can be assumed that it is an inert matrix

that is capable of maintaining the same solid/liquid dissolution interface throughout the release study. The dissolution of the pesticide in the inert matrix occurs after penetration of the solvent into the pores of the MOF, followed by slow diffusion of the pesticide from the pores.[14b] The rate-limiting step of the pesticide release from this type of system is the penetration of the solvent into the matrix, presenting a first-order kinetics, as reported in earlier studies (**Table 2**).[33] The total amount of 2,4-D released from the MOFs were calculated from the cumulative 2,4-D release over 16 days, as shown in Tables S6 and S15 (Supporting Information), showing the highest loading capacity of 45.4 wt.% for IS-2,4-D@UiO-66, followed by 22.4 wt%, 36.3 wt%, and 26.5 wt% for PS-2,4-D@UiO-66, IS-2,4-D@UiO-66-NH$_2$, and PS-2,4-D@UiO-66-NH$_2$, respectively. Attempt to determine the loading capacity have shown relatively lower release with 60 min of sonication, with IS-2,4-D@UiO-66-NH$_2$ having the highest release to yield loading capacity of 25.4 wt.%, followed by 13.8 wt%, 10.6 wt% and 10.3 wt% for IS-2,4-D@UiO-66, PS-2,4-D@UiO-66-NH$_2$, and IS-2,4-D@UiO-66-NH$_2$, respectively. These loading capacities may be due to 2,4-D being trapped into the MOF pores by strong supramolecular interactions leading to incomplete release of 2,4-D on sonication.

Numerous studies have investigated the extraction of 2,4-D from aqueous media using MOFs and have reported comparable loading capacities to this study.[34] Depending on the loading methodologies, and MOFs, the samples showed a distinct difference in the release rates. The in situ loaded UiO-66 showed a release rate 308% faster than the in situ loaded UiO-66-NH$_2$. However, the IS-2,4-D@UiO-66 had the highest % loading, which is expected as the 2,4-D molecules can occupy the octahedral and tetrahedral pores inside the UiO-66, which was further supported by the computational studies (see next section). The % loading of 2,4-D for PS-2,4-D@UiO-66 is similar to PS-2,4-D@UiO-66-NH$_2$.

The fact that UiO-66 showed faster delivery than UiO-66-NH$_2$ corroborates to the hypothesis that the hydrogen bond interactions between the carboxylate group of 2,4-D and —NH$_2$ groups of UiO-66-NH$_2$–should promote the slow release. Complementary computational studies were performed to investigate the interactions between the MOFs and 2,4-D. The slower release for the UiO-66-NH$_2$ can be attributed to higher affinity of 2,4-D molecules with the —NH$_2$ groups. For Octahedral (O_h) pores, the binding energy of 2,4-D to UiO-66-NH$_2$ is $\approx$280 kJ mol^{-1}, which is about twice compared to the binding energy for UiO-66. While for tetrahedral (T_d) pores, the binding energy of 2,4-D is $\approx$225 kJ mol^{-1} that is $\approx$50% higher than bare T_d pores of UiO-66 (140 kJ mol^{-1}) (**Figure 9**). When a second 2,4-D is introduced,

Table 2. release rate constant ($k_{release}$) using Korsmeyer–Peppas Model, release exponent (n) and the percent of pesticide loaded (wt.%) for MOFs and MOF-PCL composites.

Sample	Powder			PCL film		
	$k_{release}$ [h^{-1}]	n	%loaded	$k_{release}$ [h^{-1}]	n	%loaded
IS-2,4-D@UiO-66	0.330104	0.151278	45.4 ± 0.1	0.15578	0.320186	25.11 ± 0.004
PS-2,4-D@UiO-66	0.28228	0.141612	22.4 ± 0.3	0.120813	0.316817	29.51 ± 0.003
IS-2,4-D@UiO-66- NH$_2$	0.10738	0.3845	36.3 ± 0.3	0.058241	0.498489	34.98 ± 0.003
PS-2,4-D@UiO-66- NH$_2$	0.277656	0.189991	26.50 ± 0.02	0.254272	0.209131	23.35 ± 0.02

**ADVANCED
SCIENCE NEWS**

www.advancedsciencenews.com

**ADVANCED
SUSTAINABLE
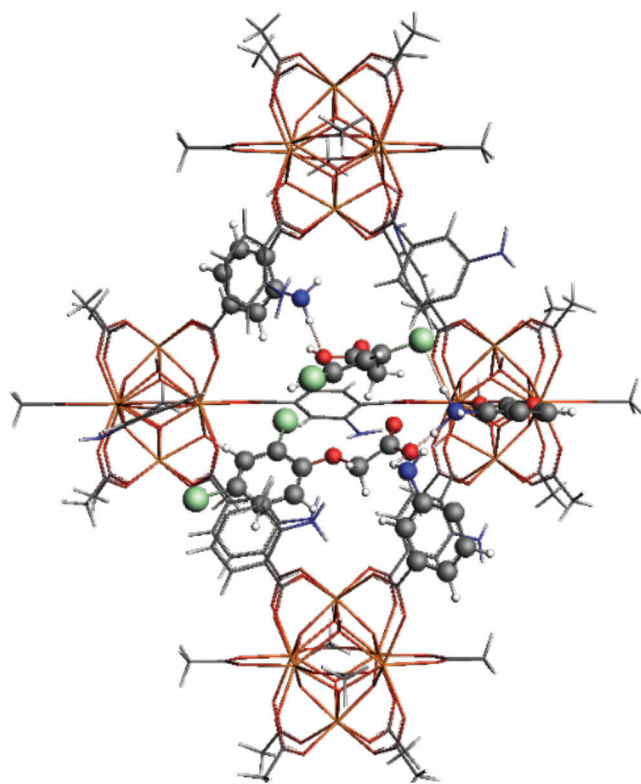SYSTEMS**

www.advsustainsys.com

Figure 9. Model showing two-guest MOF interaction for UiO-66-NH$_2$ in the octahedral pore. Dotted lines showing the H–bonds formed at this conformation between the NH$_2$ group of UiO-66-NH$_2$ and carboxylate and —Cl groups of the 2,4-D molecules.

differences in molecules stacking arise from the pore geometries. Calculations show no significant difference in binding energies between UiO-66 and —NH$_2$ functionalized UiO-66 in tetrahedral pores (see Table S19, Supporting Information). This is because the size of the tetrahedral pore is too small to accommodate both

molecules. In contrast, the effect of —NH$_2$ functionalization on binding energy can be observed in octahedral pores, as the amino groups actively form hydrogen bonds with the —Cl or —COOH groups of the 2,4-D molecules. This is in contrast to non-functionalized pores of UiO-66, where hydrogen bonding occurs only to the metal clusters.

To rule out any other mechanism of release, a blank sample with a mixture of pure reactants (2,4-D, UiO-NH$_2$) were put in water and the release was studied (Figure S10, Supporting Information). In IS-2,4-D@UiO-66-NH$_2$ release is controlled and gradual, while all the 2,4-D was totally dissolved in the blank sample in the first hour, without any control.

The 2,4-D release studies showed a controlled release profile for all the composites (**Figure 10**). The Korsmeyer–Peppas model was used to study the release kinetics. This empirical equation is commonly used to investigate both Fickian and non-Fickian release from polymeric delivery systems.[35] Fickian diffusion occurs when the rate of drug diffusion is slower than the rate of polymeric chain relaxation time,[36] that is the polymer's ability to maintain equilibrium once exposed to external force. As a result, the drug concentration gradient is the driving factor for release. While for non-Fickian diffusion, the drug diffusion rate is comparable or higher than the polymeric chain relaxation, and hence, drug concentration gradient and polymer erosion both contribute to the drug release (**Figure 11**).

After obtaining the [2,4-D]$_\infty$ from the calibration curve (Figure S2, Supporting Information), the kinetic fitting was adjusted to minimize the sum of the squares of the deviations. By using [2,4-D]$_\infty$ = [2,4-D]$_{384\,h}$, the k$_{release}$ was calculated. The kinetic parameters and correlation coefficient of the Korsmeyer–Peppas model can be found in Tables S9 and S16 (Supporting Information). To determine the exponent n, only the portion where $\frac{[2,4-D]_t}{[2,4-D]_\infty} < 0.6$ were used. The value of n >0.45 indicates a classical Fickian pure diffusion-controlled release.

For all powder releases studied, the behavior is a Fickian diffusion (n<0.45). When the polymeric chain relaxation time is much greater than the characteristic solvent diffusion time, the
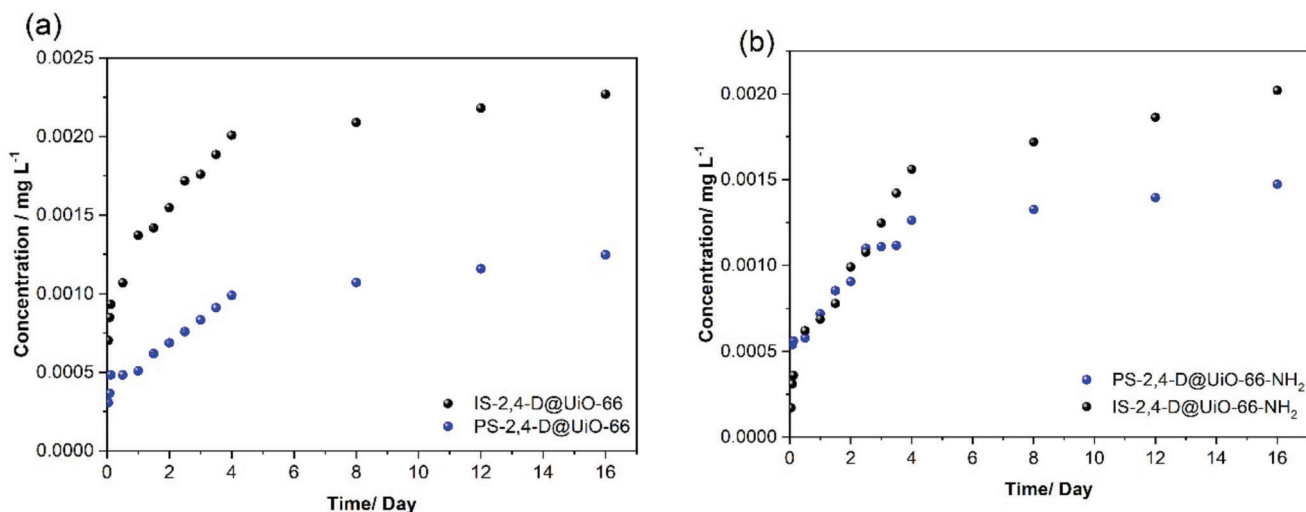

Figure 10. Release studies of 2,4-D loaded MOFs in water over a period of 16 days for in situ and post-synthetically loaded a) UiO-66 samples, and b) UiO-66-NH$_2$ samples.
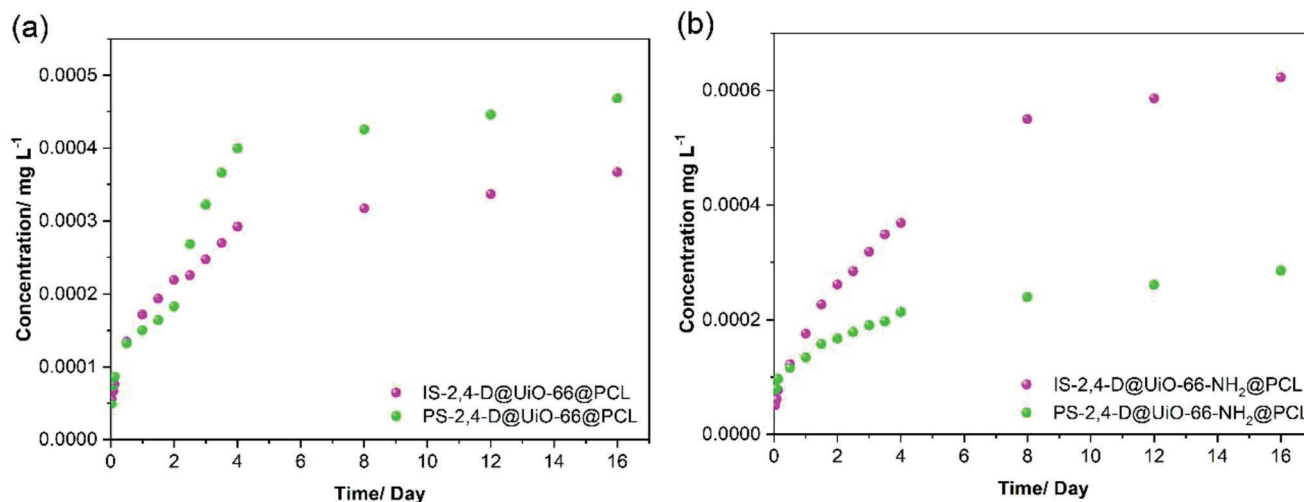
**ADVANCED
SCIENCE NEWS**

www.advancedsciencenews.com

**ADVANCED
SUSTAINABLE
SYSTEMS**

www.advsustainsys.com

Figure 11. Release studies of 2,4-D loaded MOF-PCL composites in water over a period of 16 days for a) UiO-66 samples, b) UiO-66-NH$_2$ samples.

behavior for all release mechanisms is characterized by Fickian diffusion, as indicated by a value of n < 0.45. In this scenario, solute transport is mainly driven by the concentration gradient of the solute, rather than the interaction between the polymer and solvent.[37] For PCL composites IS- 2,4-D@UiO-66@PCL, PS-2,4-D@UiO-66@PCL, and PS-2,4-D@UiO-66-NH$_2$@PCL release studies show n >0.45, indicating release mechanism classified as non swellable matrix-diffusion.[14a] For IS- 2,4-D@UiO-66-NH$_2$@PCL, as 0.45 < n < 0.89, the transport mechanism could be related a non-Fickian, a release mechanism where the diffusion in the hydrated matrix and the polymer relaxation occurs simultaneously.[37,14a] Finally, as the release is governed by Fick's first law, the presence of one more polymer matrix (PCL) in the system alters the diffusion-rate constants found.

$$\frac{[2,4-D]_t}{[2,4-D]_\infty} = k * t^n \tag{7}$$

4. Conclusion

In conclusion, a widely used pesticide 2,4-D was loaded into UiO-66 and UiO-66-NH$_2$ using post-synthetic and in situ methods, and the loaded MOFs were further integrated into biodegradable polycaprolactone membranes. The 2,4-D release behavior were studied in water and the PCL composites of PS-2,4-D@UiO-66 and IS- 2,4-D@UiO-66- NH$_2$ showed promising loading capacities, reaching loading capacity up to 45 wt.% for IS-2,4-D@UiO-66-NH$_2$. The 2,4-D-loaded MOFs were incorporated into biodegradable polycaprolactone composites for convenient handling and integration into biodegradable membranes that can be potentially used in agricultural setup. It was observed that even in direct contact with water, the release of the pesticide is long-lasting, and sustainable, indicating the potential for practical agricultural applications of the MOF-polymer composites for controlled and sustainable delivery of pesticides or other agrochemicals. This approach will facilitate delivery of the pesticide to the sites in contact with the weeds, while minimizing pesticide contamination to non-targeted organisms and the surrounding environment, providing a new approach for a cleaner, controlled

and more sustained delivery of pesticides. As obvious next steps, further studies are planned for investigating the viability, optimization and upscaling of the composite materials, and their effect on crop models.

Supporting Information

Supporting Information is available from the Wiley Online Library or from the author.

Conflict of Interest

The authors declare no conflict of interest.

Author Contributions

R.A.D.R. and L.A.M.M. contributed equally to this work. R.A.R. and L.A.A.M performed implementation of idea, experiments, materials characterization, and preparation of manuscript. E.H.I. performed experiments, materials characterization, and preparation of manuscript. R.T. performed conceptualization, review, and editing manuscript. M.A.A. performed computational studies, review, and editing of manuscript. L.R.T. performed investigation (materials characterization) analysis, review, and editing manuscript. V.P.T. performed supervision, review, and editing of manuscript. S.N. performed project lead, conceptualization, supervision, materials characterization, review, editing, and submission of manuscript.

Data Availability Statement

The data that support the findings of this study are available from the corresponding author upon reasonable request.

[1] A. K. Chopra, M. K. Sharma, S. Chamoli, *Environ Monit Assess* **2011**, *173*, 905.

[2] C. A. Brühl, J. G. Zaller, *Front. Environ. Sci.* **2019**, *7*, 75.

[3] P. Nicolopoulou-Stamati, S. Maipas, C. Kotampasi, P. Stamatis, L. Hens, *Front Public Health* **2016**, *4*, 148.

[4] I. Boughattas, N. Zitouni, S. Hattab, M. Mkhinini, O. Missawi, S. Helaoui, M. Mokni, N. Bousserrhine, M. Banni, *J. Hazard. Mater.* **2022**, *424*, 127578.

[5] a) S. M. Li, F. Feng, S. Chen, X. L. Zhang, Y. X. Liang, S. S. Shan, *Ecotox. Environ. Safe* **2020**, *194*, 6; b) M. F. Yorlano, P. M. Demetrio, F. Rimoldi, *Sci. Total Environ.* **2022**, *807*, 150655.

[6] a) I. El-Nahhal, Y. El-Nahhal, *J Environ Manage* **2021**, *299*, 113611; b) X. Wu, A. Chen, Z. Yuan, H. Kang, Z. Xie, *Chemosphere* **2020**, *258*, 127359.

[7] a) M. Chandel, K. Kaur, B. K. Sahu, S. Sharma, R. Panneerselvam, V. Shanmugam, *Carbon* **2022**, *188*, 461; b) M. Anstoetz, T. J. Rose, M. W. Clark, L. H. Yee, C. A. Raymond, T. Vancov, *PLoS One* **2015**, *10*, e0144169.

[8] S. R. Batten, N. R. Champness, X.-M. Chen, J. Garcia-Martinez, S. Kitagawa, L. Öhrström, M. O'keeffe, M. Paik Suh, J. Reedijk, *Pure Appl. Chem.* **2013**, *85*, 1715.

[9] O. M. Yaghi, H. Li, *J. Am. Chem. Soc.* **1995**, *117*, 10401.

[10] L. Yang, X. F. Zeng, W. C. Wang, D. P. Cao, *Adv. Funct. Mater.* **2018**, *28*, 21.

[11] J. Ren, H. W. Langmi, B. C. North, M. Mathe, *Int. J. Energy Res.* **2015**, *39*, 607.

[12] J. Lee, O. K. Farha, J. Roberts, K. A. Scheidt, S. T. Nguyen, J. T. Hupp, *Chem. Soc. Rev.* **2009**, *38*, 1450.

[13] a) J. An, S. J. Geib, N. L. Rosi, *J. Am. Chem. Soc.* **2009**, *131*, 8376; b) F. Li, Y. Qin, J. Lee, H. Liao, N. Wang, T. P. Davis, R. Qiao, D. Ling, *J. Controlled Release* **2020**, *322*, 566; c) S. S. Al Neyadi, A. G. Al Blooshi, H. L. Nguyen, M. A. Alnaqbi, *New J. Chem.* **2021**, *45*, 20386; d) R. C. Alves, Z. M. Schulte, M. T. Luiz, P. Bento Da Silva, R. C. G. Frem, N. L. Rosi, M. Chorilli, *Inorg. Chem.* **2021**, *60*, 11739; e) Q. He, J. Shen, X. H. Guan, Y. B. Han, X. Y. Jiang, X. Shen, X. J. Huang, Y. F. Chen, C. Lei, X. Y. Xiao, W. X. Lin, *Z. Anorg. Allg. Chem.* **2022**, *648*, 5; f) S. Mallakpour, E. Nikkhoo, C. M. Hussain, *Coord. Chem. Rev.* **2022**, *451*, 214262.

[14] a) C. Yin, X. Li, *Int. J. Pharm.* **2011**, *418*, 78; b) A. Talevi, M. E. Ruiz, in *The ADME Encyclopedia: A Comprehensive Guide on Biopharmacy and Pharmacokinetics*, Springer, Cham **2021**.

[15] a) A. Derylo-Marczewska, M. Blachnio, A. W. Marczewski, A. Swiatkowski, B. Tarasiuk, *J. Therm. Anal. Calorim.* **2010**, *101*, 785; b) F.

[16] L. A. M. Mahmoud, R. A. Dos Reis, X. Chen, V. P. Ting, S. Nayak, *ACS Omega* **2022**, *7*, 45910.

[17] a) Y. Ma, R. Zhao, H. Shang, S. Zhen, L. Li, X. Guo, M. Yu, Y. Xu, J. Feng, X. Wu, *ACS Appl. Nano Mater.* **2022**, *5*, 11864; b) M. Wan, S. Song, W. Feng, X. Wang, J. Shen, *ACS Appl. Eng. Mater.* **2023**, *1*, 1079.

[18] J. Yang, C. A. Trickett, S. B. Alahmadi, A. S. Alshammari, O. M. Yaghi, *J. Am. Chem. Soc.* **2017**, *139*, 8118.

[19] N. M. Ranjha, J. Mudassir, S. Majeed, *Bull. Mater. Sci.* **2011**, *34*, 1537.

[20] M. A. Addicoat, S. Fukuoka, A. J. Page, S. Irle, *J. Comput. Chem.* **2013**, *34*, 2591.

[21] a) D. E. Coupry, M. A. Addicoat, T. Heine, *J. Chem. Theory Comput.* **2016**, *12*, 5215; b) M. A. Addicoat, N. Vankova, I. F. Akter, T. Heine, *J. Chem. Theory Comput.* **2014**, *10*, 880.

[22] S. Grimme, C. Bannwarth, P. Shushkov, *J. Chem. Theory Comput.* **2017**, *13*, 1989.

[23] ADF2017, SCM, *Theoretical Chemistry*, Vrije Universiteit, Amsterdam, The Netherlands, Available online: http://www.scm.com.

[24] G. H. Huang, Y. F. Deng, Y. C. Zhang, P. Feng, C. H. Xu, L. H. Fu, B. F. Lin, *Chem. Eng. J.* **2021**, *403*, 11.

[25] M. Thommes, K. Kaneko, A. V. Neimark, J. P. Olivier, F. Rodriguez-Reinoso, J. Rouquerol, K. S. W. Sing, *Pure Appl. Chem.* **2015**, *87*, 1051.

[26] C. A. Trickett, K. J. Gagnon, S. Lee, F. Gándara, H.-B. Bürgi, O. M. Yaghi, *Angew. Chem., Int. Ed.* **2015**, *54*, 11162.

[27] M. J. Katz, Z. J. Brown, Y. J. Colón, P. W. Siu, K. A. Scheidt, R. Q. Snurr, J. T. Hupp, O. K. Farha, *Chem. Commun.* **2013**, *49*, 9449.

[28] M. Athar, P. Rzepka, D. Thoeny, M. Ranocchiari, J. Anton Van Bokhoven, *RSC Adv.* **2021**, *11*, 38849.

[29] S. Atta, A. Paul, R. Banerjee, M. Bera, M. Ikbal, D. Dhara, N. D. P. Singh, *RSC Adv.* **2015**, *5*, 99968.

[30] Y. Cao, H. Zhang, F. Song, T. Huang, J. Ji, Q. Zhong, W. Chu, Q. Xu, *Materials* **2018**, *11*, 589.

[31] O. Persenaire, M. Alexandre, P. Degée, P. Dubois, *Biomacromolecules* **2001**, *2*, 288.

[32] X. Liu, N. K. Demir, Z. Wu, K. Li, *J. Am. Chem. Soc.* **2015**, *137*, 6999.

[33] M. V. S. Varma, A. M. Kaushal, A. Garg, S. Garg, *Am. J. Drug Deliv.* **2004**, *2*, 43.

[34] a) B. Y. Liu, N. D. Guo, Z. Wang, Y. Wang, X. Hao, Z. L. Yang, Q. Yang, *J. Environ. Chem. Eng.* **2022**, *10*, 12; b) M. Sarker, I. Ahmed, S. H. Jhung, *Chem. Eng. J.* **2017**, *323*, 203; c) G. G. Wu, J. P. Ma, S. Li, S. S. Wang, B. Jiang, S. Y. Luo, J. H. Li, X. Y. Wang, Y. F. Guan, L. X. Chen, *Environ. Res.* **2020**, *186*, 9.

[35] P. Sriamornsak, N. Thirawong, Y. Weerapol, J. Nunthanid, S. Sungthongjeen, *Eur. J. Pharm. Biopharm.* **2007**, *67*, 211.

[36] I. Y. Wu, S. Bala, N. Skalko-Basnet, M. P. Di Cagno, *Eur. J. Pharm. Sci.* **2019**, *138*, 105026.

[37] Y. Fu, W. J. Kao, *Expert Opin. Drug Delivery* **2010**, *7*, 429.

J. R. Mejías, S. Trasobares, R. M. Varela, J. M. G. Molinillo, J. J. Calvino, F. A. Macías, *ACS Appl. Mater. Interfaces* **2021**, *13*, 7997; c) L. A. M. Mahmoud, R. Telford, T. C. Livesey, M. Katsikogianni, A. L. Kelly, L. R. Terry, V. P. Ting, S. Nayak, *ACS Appl Bio Mater* **2022**, *5*, 3972; d) S. X. Lee, G. H. Wang, N. N. Ji, M. Zhang, D. Wang, L. S. Sun, W. Q. Meng, Y. Q. Zheng, Y. X. Li, Y. T. Wu, *Z. Anorg. Allg. Chem.* **2022**, *648*, 11.